




Cite this: *Green Chem.*, 2023, **25**, 7259

Dibasic esters as green solvents for PVDF membrane preparation†

Norafiqah Ismail,^a Qiuyueming Zhou,^b Qian Wang,^b Zhaoliang Cui,^b Nils Skoglund^c and Naser Tavajohi *^a

Solvent toxicity is a major barrier to sustainable fabrication of polymeric membranes. This study introduces three dibasic esters (DBEs) as alternative membrane fabrication solvents that are biodegradable, non-carcinogenic, non-corrosive, and non-hazardous. The use of DBEs in fabrication processes shifts the monotectic point in the phase diagram of PVDF/solvent systems towards higher polymer concentrations, enabling membrane formation by liquid–liquid phase inversion to produce a bicontinuous structure that confers outstanding performance. The best-performing membrane prepared in this way had an exceptional flux of 42.40 kg m^{−2} h^{−1} and a high rejection rate (>99%) in the decontamination of synthetic nuclear wastewater. Compared to membranes prepared previously using toxic and non-toxic solvents, membranes fabricated in DBEs exhibited superior mechanical performance due to their bicontinuous structure, which effectively distributes external forces throughout the membrane. Moreover, DBEs are cheaper than toxic conventional solvents and are readily available in bulk, making them attractive options for industrial-scale membrane production.

Received 1st July 2023,
Accepted 14th August 2023

DOI: 10.1039/d3gc02366d

rsc.li/greenchem

1. Introduction

Nuclear power plants account for 10% of global electricity generation and produce minimal lifecycle carbon emissions.¹ However, the growing accumulation of nuclear waste, including contaminated wastewater,² poses significant risks to the environment and human health. Radioactive wastewater is typically treated using conventional methods such as chemical precipitation, evaporation, and electrochemical processes.^{3,4} However, these techniques are limited in that they cannot remove all contaminants in a single step and therefore generate secondary waste that increases operational expenses.⁵

The most common physicochemical methods for treating radioactive wastewater are adsorption and ion exchange. These methods effectively reduce radioactivity levels by targeting the major nuclides in the wastewater, specifically ¹³⁴Cs and ¹³⁷Cs.⁶ The advantage of such methods lies in their use of readily available and cost-effective adsorbents such as zeolite, kaolin, and activated carbon. However, these materials have some

limitations including low adsorption rates, low adsorption capacities, and limited reusability.⁷

Membrane processes have emerged as a promising alternative for removing radionuclides with distinct advantages over conventional methods. Conventional membrane processes include microfiltration, ultrafiltration, and nanofiltration, all of which offer simplicity, operational ease, low energy consumption, high decontamination efficiency, and compatibility with other processes.⁵ However, a significant limitation of these pressure-driven processes is that they cannot completely reject radionuclides and the membranes are prone to fouling issues.³

Membrane distillation (MD) is an alternative thermally driven separation process that has drawn attention as an option for decontaminating low- and intermediate-level radioactive liquid wastes in recent years.^{5,8–13} MD has several favorable characteristics, including high separation efficiency with a theoretical separation factor of 100%, mild operating conditions, low fouling tendency, and the ability to utilize waste heat from nuclear reactors.⁵

The membrane's performance and stability strongly affect the effectiveness of MD processes. An ideal MD membrane should have high hydrophobicity and pore connectivity as well as good porosity and a narrow pore size distribution.¹⁴ MD membranes are generally made from fluoropolymers such as polyvinyl difluoride (PVDF), ethylene-chlorotrifluoroethylene (ECTFE), and polytetrafluoroethylene (PTFE) due to their favorable physicochemical properties and high hydrophobicity

^aDepartment of Chemistry, Umeå University, 90187 Umeå, Sweden.

E-mail: naser.tavajohi@umu.se

^bState Key Laboratory of Materials-Oriented Chemical Engineering, College of Chemical Engineering, Nanjing Tech University, Nanjing 211816, PR China

^cDepartment of Applied Physics and Electronics, Umeå University, 90187 Umeå, Sweden

†Electronic supplementary information (ESI) available. See DOI: <https://doi.org/10.1039/d3gc02366d>



relative to non-fluorinated polymers such as polysulfone (PS), polyethersulfone (PES), and polyvinyl chloride (PVC).¹⁵ PVDF is the most commonly used fluoropolymer for MD membrane fabrication because of its cost-effectiveness and solution processability,¹⁶ the latter of which allows membranes to be fabricated using the phase inversion method.¹⁷ While this method is used extensively in both academic and industrial membrane fabrication, currently used solvents for PVDF membrane production have several drawbacks.

The choice of solvent affects both the kinetics and the thermodynamics of phase inversion, and therefore influences the properties and performance of the fabricated membrane. Unfortunately, most solvents currently used for PVDF membrane fabrication are toxic and have negative effects on both human health and the environment. Accordingly, a recent study found that solvent toxicity is the main barrier to sustainable fabrication of polymeric membranes including PVDF membranes.¹⁸ Consequently, a number of environmentally friendly solvents have been introduced as alternatives to toxic conventional solvents for membrane fabrication. Prominent examples include methyl-5-(dimethylamino)-2-methyl-5-oxopentanoate (Polarclean®),¹⁹ dihydrolevoglucosenone (Cyrene™), tributyl *O*-acetyl citrate (ATBC),^{20,21} and citric acid esters.²² Methyl esters have drawn particular interest in this context (as outlined in Table 1) because their low toxicity and

high boiling points are both favorable for membrane fabrication.

To our knowledge, all green solvents that have been tested in PVDF membrane fabrication to date only dissolve PVDF at elevated temperatures, necessitating a thermally induced phase separation (TIPS) membrane fabrication method. Some of these solvents, like ATBC, are insoluble in water, meaning that phase inversion can only occur *via* a TIPS mechanism.²³ However, other solvents such as Polarclean and cyclic carbonates are soluble in the quenching medium (which is typically water), allowing phase separation to occur *via* a combination of thermally- and nonsolvent-induced mechanisms.^{19,24} Detailed information on phase inversion methods and mechanisms in PVDF membrane fabrication can be found in a recently published review article.²⁵

Controlling membrane morphology is vitally important in membrane fabrication processes because it directly influences overall membrane performance. Literature data show that for TIPS processes, membranes with a bicontinuous morphology have greater mechanical strength and better pore connectivity than those with cellular or spherulitic structures, assuming an equal polymer content. However, achieving a bicontinuous morphology in TIPS-based fabrication processes is challenging because it requires phase separation by spinodal decomposition, which typically occurs only if the polymer-solvent com-

Table 1 Prepared membranes using fluoropolymers and methylated solvents

Polymer	Solvent		Hazard	Boiling point (°C)	Configuration	Ref.
	Type	Properties				
PVDF	ATEC	Water soluble solvent	H319	228–229	FS	22
PVDF	DCAC	Clear liquid, colorless		218	FS	26
PVDF	TBC	Clear and viscous liquid		225	FS	27
ECTFE	TEC	Clear liquid, light yellow color		294	HF	28
PVDF					FS	22
PVDF	ATBC	Colorless, slight and sweet odor, soluble in organic solvents		327	FS & HF	20
					HF	21
					FS	22
PVDF/PMMA	GTA	Clear liquid, colorless, fatty odor		258–260	HF	29
PVDF					HF	30
					HF	31
					HF	32 and 33
PVDF	TEGDA	Colorless, odorless	H302, H315, H319, H335	286	FS	34
PVDF	Polarclean	Clear, slightly yellow liquid	H317, H373, H411	278–282	HF	19
PVDF	DBM	Clear, virtually colorless liquid, ester-like odor		281	FS	35
ECTFE	TOTM	Viscous, light yellow color		414	FS	36
PVDF	TEP	Clear liquid, colourless, odorless	H302, H319	215	FS	37
					HF	38
PVDF	γ-BL	Clear liquid, colorless, unpleasant odor	H302, H318, H336	204	HF	39
PVDF	DMS	High water-soluble solvent, colorless liquid,	H319	200	FS	This study
	DMG	biodegradable	—	216		
	DMA		H319	227		

ATEC: acetyl triethyl citrate, DCAC: diethyleneglycol monoethyl ether acetate, TBC: tributyl citrate, TEC: triethyl citrate, ATBC: tributyl *O*-acetyl citrate, GTA: glycerol triacetate, TEGDA: triethylene glycol diacetate, Polarclean: methyl-5-(dimethylamino)-2-methyl-5-oxopentanoate, DBM: maleic acid dibutyl ester, TOTM: trioctyl trimellitate, TEP: triethyl phosphate, γ-BL: γ-butyrolactone, DMS: dimethyl succinate, DMG: dimethyl glutarate, DMA: dimethyl adipate, FS: flat sheet, HF: hollow fiber. Hazard codes: H302: harmful if swallowed, H315: causes skin irritation, H317: may cause an allergic skin reaction, H318: causes serious eye damage, H319: causes serious eye irritation, H335: may cause respiratory irritation, H336: may cause drowsiness, H373: may cause damage to organ, H411: toxic to aquatic life with long lasting effects.



patibility is moderate and the polymer concentration is low (below the monotectic point).

The use of solutions with low polymer concentrations often yields membranes with insufficient mechanical strength. Increasing the polymer concentration increases mechanical integrity but can cause the final membrane to adopt a spherulitic structure instead of the desired bicontinuous morphology. This could be avoided by identifying a polymeric system with an elevated monotectic point that would undergo liquid-liquid (L-L) phase separation at high polymer concentrations. Researchers studying TIPS processes have therefore sought to identify solvents with broader binodal curves but have achieved only limited success. This has prompted some groups to redirect their focus towards binary or mixed solvent systems to more effectively control the breadth of the binodal curve.²⁵

Dibasic esters (DBE) are methylated solvents that are non-carcinogenic, non-corrosive, non-hazardous, of low toxicity, and not volatile organic compounds (VOCs).⁴⁰ Three DBEs, namely dimethyl succinate (DMS), dimethyl glutarate (DMG), and dimethyl adipate (DMA), are available on commercial scales and are used as plasticizers, coating materials, paint removers, and resin/polymer cleaning solvents among other things. The size of the DBE market was estimated to be around \$440.9 million in 2021 and it is projected to grow by 42.4% by 2028. Consequently, DBEs are readily available on large scales globally.⁴¹

To date, there have been no publications on membrane formation using DBEs. However, some studies have focused on the production of thermoreversible gels of PVDF and various organic diesters $[(CH_2)_n - (COOEt)_2]$ by Dikshit *et al.*^{42,43} In addition, Dasgupta and Nandi introduced different diester groups, namely diethyl adipate, diethyl suberate, and diethyl azelate, to produce micro- and mesoporous PVDF membranes suitable for separating impurities of different sizes (ranging from nano to macro) and different chemical properties.⁴⁴

This study describes the fabrication of PVDF membranes using three biodegradable methylated solvents from the DBE family: DMS, DMG, and DMA. The membranes were fabricated *via* a TIPS process requiring no additives, membrane supports, or modification steps. All three solvents are shown to yield

broad binodal curves, allowing L-L phase separation to occur over a wide range of polymer concentrations. The prepared membranes were tested by evaluating their efficiency in decontaminating synthetic nuclear wastewater using an MD process. Remarkably, the utilization of the aforementioned solvents endowed the fabricated membranes with an interconnected structure, leading to interesting properties of high flux, rejection, and mechanical strength. The remarkable synergistic combination of high flux and rejection observed in this study suggests that methylated DBE solvents have great potential for fabricating PVDF membranes with interconnected structures that could be tremendously valuable in MD processes, particularly for the efficient treatment of nuclear wastewater.

2. Methodology

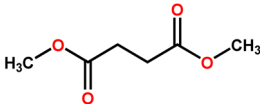
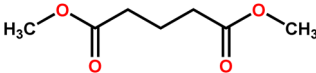
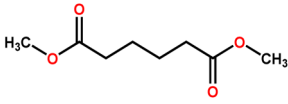
2.1. Materials

The PVDF polymer (Solef 1015, $M_w = 534\,000\text{ g mol}^{-1}$) was generously provided by Solvay Specialty Polymers. The solvents used in this work, namely dimethyl succinate (DMS), dimethyl glutarate (DMG), and dimethyl adipate (DMA), were procured from Sigma Aldrich. Their properties are listed in Table 2. Ethanol with a purity of 96% was acquired from VWR International. Salts used in the filtration experiment, namely sodium chloride (NaCl, $M_w = 58.44\text{ g mol}^{-1}$), sodium nitrate (NaNO_3 , $M_w = 84.99\text{ g mol}^{-1}$), cesium chloride (CsCl , $M_w = 168.36\text{ g mol}^{-1}$), cobalt(II) nitrate hexahydrate ($\text{Co}(\text{NO}_3)_2 \cdot 6\text{H}_2\text{O}$, $M_w = 291.03\text{ g mol}^{-1}$), strontium chloride hexahydrate ($\text{SrCl}_2 \cdot 6\text{H}_2\text{O}$, $M_w = 266.62\text{ g mol}^{-1}$) were procured from Sigma Aldrich. All chemicals were used as supplied without further purification.

2.2. Membrane fabrication

Dope solutions were prepared by adding PVDF to each of the three tested solvents (DMA, DMG, and DMS) at a fixed concentration of 18 wt%. The solutions were then stirred continuously at 110 °C until they became homogeneous and transparent. Flat sheet membranes with a fixed thickness of 300 μm were then cast at a casting temperature of 50 °C. After casting, the nascent membranes were immersed in a coagulation bath

Table 2 Properties of solvents used in this study

Properties	DMS	DMG	DMA
Chemical structure			
Molecular weight (g mol^{-1})	146.14	160.17	174.2
Melting point ($^{\circ}\text{C}$)	16–19	–38	8
Boiling point ($^{\circ}\text{C}$)	200	216	227
Density (g cm^{-3})	1.117	1.09	1.06
Water solubility (g l^{-1})	122.9	63.1	25
Hazard statements	H319	—	H319

H319 – causes serious eye irritation.



of 30% ethanol in distilled water for 5 minutes before being transferred to a coagulation bath filled with water and left to soak for 1 day to extract the residual solvent. The membranes prepared using DMS, DMG, and DMA are denoted as PVDF/DMS, PVDF/DMG, and PVDF/DMA, respectively.

2.3. Solubility parameter

The solubility parameter, δ reflects the contributions of the dispersive interaction (δ_d), the polar interaction between permanent dipoles (δ_p), and hydrogen bonding to solubility. The solubility parameters of each solvent used in this study were calculated using the group contribution method as described in an earlier publication.⁴⁵ The solubility distance parameter, Ra , was calculated using the following expression:

$$Ra = [4(\delta_{d,p} - \delta_{d,s})^2 + (\delta_{p,p} - \delta_{p,s})^2 + (\delta_{h,p} - \delta_{h,s})^2]^{0.5} \quad (1)$$

The polymer-solvent interaction parameter was calculated using the Flory-Huggins interaction parameter, which was expanded by incorporating the Hansen solubility parameter using the following equation:

$$\chi = \frac{V_s}{RT} [(\delta_{d,p} - \delta_{d,s})^2 + 0.25(\delta_{p,p} - \delta_{p,s})^2 + 0.25(\delta_{h,p} - \delta_{h,s})^2] \quad (2)$$

Here, V_s represents the solvent's molar volume, while δ_p and δ_s are the solubility parameters of the polymer and solvent respectively. R denotes the gas constant ($8.3145 \text{ J mol}^{-1} \text{ K}^{-1}$) and T represents the temperature in K.

2.4. Characterization

The phase diagram is a key tool for understanding the thermodynamics of phase separation. In this study, phase diagrams were constructed for multiple polymer/solvent systems with five polymer concentrations ranging from 10 wt% to 30 wt% which is a typical PVDF concentration range for fabricating flat sheet and hollow fiber membranes.^{19,20,25,39,46} The cloud point was determined using a polarizing microscope by placing a minute quantity of the polymer solution between microscope slides. The sample was then heated to 200 °C and held at this temperature for 5 minutes until the polymer solution was completely molten. It was then cooled to room temperature at a controlled rate of 6 °C min⁻¹. The cloud point temperature was recorded as the temperature at which circular or snowflake-like bright spots were first observed. To ensure accuracy, measurements were repeated five times to obtain the average temperature.

The crystallization temperature was assessed using differential scanning calorimetry (DSC, Q20). A sample weighing 5 mg was subjected to controlled heating to 200 °C at a rate of 10 °C min⁻¹. It was then briefly held at this temperature before being cooled at 10 °C min⁻¹. The temperature at which the exothermic peak reached its maximum was recorded as the crystallization temperature.

Fourier transformation infrared (FTIR) spectra were acquired using a Bruker Vertex 80 spectrometer operating in

attenuated total reflection (ATR) mode. The spectral range extended from 400 to 1600 cm⁻¹ with a resolution of 2 cm⁻¹.

X-ray diffraction analysis (XRD) was performed using a PANalytical X'Pert PRO X-ray diffractometer operating at 40 kV and 40 mA with a Cu-K α radiation wavelength of 0.154 nm. A slit size of 1/2° was used for all measurements and samples were scanned in reflection mode within the 2θ range of 10° to 40° at a scanning rate of 0.3° min⁻¹.

The membrane surface and cross-sectional structures were analyzed using a field emission scanning electron microscope (FE-SEM). To obtain clear cross-section images, the samples were freeze-fractured in liquid nitrogen before being coated with a 5 nm thick palladium layer using a Quorum Q150T-ES Sputter Coater.

The membrane thickness was measured using a digital micrometer. Five measurements were taken at different spots on the membrane and the resulting measurements were averaged.

The membranes' liquid entry pressure (LEP) was determined using a dead-end filtration cell. Pure water was pushed against one face of the membrane by gradual pressurization with nitrogen gas, increasing the pressure at a rate of 0.2 bar. The LEP was then recorded as the pressure at which the first droplet was observed on the membrane face opposite the water.

The overall porosity (ϵ) was determined using a gravimetric method. The membranes were weighed in a dry state (m_d) and after being immersed in kerosene for 1 day (wet state, m_w). The overall porosity was then calculated using the following equation:

$$\epsilon(\%) = \frac{(m_w - m_d)/\rho_k}{(m_w - m_d)/\rho_k + m_d/\rho_p} \times 100 \quad (3)$$

Here, ρ_k is the density of kerosene (0.81 g cm⁻³) and ρ_p is the density of the PVDF polymer (1.78 g cm⁻³).

The contact angle, *i.e.*, the angle between the tangent to a water droplet and the surface of the membrane, was measured using the sessile drop method with an Ossila contact angle goniometer. In brief, a 3 μ L water droplet was placed on the membrane surface and imaged at high resolution to determine the contact angle. To obtain reliable and statistically significant results, the measurements were repeated at least five times at different locations on the membrane. The mean contact angle was then determined, providing a representative measurement of the membrane's wetting behavior and surface properties.

Atomic Force Microscopy (AFM) was performed using a Dimension ICON system (Bruker, USA) to assess the morphological characteristics of membrane samples. AFM experiments were conducted at room temperature with a relative humidity of approximately 50% using tapping mode imaging with sharp silicon tips (RTESPA-300) having well-defined spring constants of $40 \pm 5 \text{ N m}^{-1}$.

The gas-liquid replacement method was used to determine the membranes' pore size distribution. Briefly, membranes



were wetted by immersion in a wetting liquid (GQ-16) with a surface tension of 16.0 dyne per cm and then mounted in the sample module of a PSDA-20 membrane pore size distribution measurement instrument (Gaoqian Function Co., Nanjing, China). Nitrogen gas was then introduced into the module at a pressure of 0.05 MPa. The acquired data, including bubble point and pore size measurements, were analyzed using custom software developed in-house.

The mechanical properties of the PVDF membranes were characterized by measuring their tensile strength and elongation at break. The thickness of the flat sheet membranes was first measured using a thickness gauge. A rectangular membrane sample with a length of 5 cm and a width of 0.5 cm was then tested in a tensile stress-strain meter (SH-20, SUNDOO, China). After recording the sample's initial length (L_0), it was slowly elongated at a constant speed until it reached the point of fracture. The length of the membrane (L) and the corresponding tensile force (F) displayed on the tensimeter were recorded at the moment of rupture. This test was performed three times on membranes prepared under identical conditions.

Tensile strength (σ) was calculated using the following equation:

$$\sigma(\text{MPa}) = \frac{F}{A} \quad (4)$$

The elongation at break (ϵ) was calculated as follows:

$$\epsilon(\%) = \frac{L - L_0}{L_0} \times 100 \quad (5)$$

2.5. Membrane distillation experiments

Air gap membrane distillation (AGMD) experiments were conducted using a laboratory-scale setup with a stainless steel flat sheet module (model CPR920, Convergence Industry B.V., Netherlands). In this module, the membrane is placed in between two chambers, one on the feed side and one on the permeate side. During the experiments, the permeate inlet temperature ($T_{p, \text{in}}$) was maintained at 20 °C, while the feed inlet temperature ($T_{f, \text{in}}$) was varied between 50 and 80 °C. The feed solutions used were aqueous solutions of NaCl (35 g L⁻¹). The feed and permeate flow rates were maintained at a constant value of approximately 1.50 L min⁻¹. The membrane flux was calculated using the following equation:

$$J(\text{kg m}^{-2} \text{h}^{-1}) = \frac{V}{At} \quad (6)$$

where V is the permeate collected in kg, A is the membrane effective area (m²), and t is the time taken in hours.

The conductivity of the feed and permeate solutions was measured using a conductivity meter (edge, model HI2003, Hanna Instruments Inc., USA). The salt concentration and salt rejection factor (α) were then determined using the following equation:

$$\alpha(\%) = \left(1 - \frac{C_f}{C_p}\right) \times 100 \quad (7)$$

where C_f and C_p are the concentrations of the bulk feed and permeate solutions, respectively. All of the prepared membranes (PVDF/DMS, PVDF/DMG, PVDF/DMA) were first tested in an AGMD configuration. The membrane that achieved the best performance in the AGMD experiments in terms of flux and salt rejection was selected for further testing in a direct contact membrane distillation (DCMD) configuration using four feed solutions: distilled water, a 35 g L⁻¹ NaCl solution, a 35 g L⁻¹ NaNO₃ solution, and simulated nuclear wastewater (SNWW). To mimic the chemical composition and physico-chemical properties of real-world nuclear wastewater, the SNWW solution contained CsCl (Cs⁺), Co(NO₃)₂·6H₂O (Co²⁺) and SrCl₂·6H₂O (Sr²⁺) at concentrations of approximately 100 ppm each in 35 g L⁻¹ NaNO₃. To assess the membrane's performance, the concentrations of Cs⁺, Co²⁺ and Sr²⁺ in the feed and permeate solutions were determined using inductively coupled plasma optical emission spectroscopy (ICP-OES) with an Agilent 5800 instrument. ICP-OES enables accurate quantification and identification of trace elements by analyzing the emission spectra generated from the sample. The nuclide rejection value was calculated as follows:

$$\text{Rejection}(\%) = \left(1 - \frac{C_f}{C_i}\right) \times 100 \quad (8)$$

where C_f is the final concentration of nuclides in the permeate and C_i is the initial concentration of nuclides in the feed side in ppm.

3. Results and discussion

3.1. Solubility of PVDF in dibasic ester solvents

The mutual compatibility between PVDF and the tested solvents was evaluated by calculating two key parameters: the Hansen solubility distance parameter (R_a) and the Flory–Huggins interaction parameter (χ). In both cases, a lower value of the parameter indicates greater compatibility between the polymer and the solvent. The values of these parameters for PVDF in the three dibasic ester solvents are provided in Table 3.

The three dibasic ester solvents have similar molecular structures, differing only in the number of methylene units in their backbones. However, these relatively minor differences had clear effects on their solubility parameters and solvation power: DMS, which has the shortest alkyl chain, had the lowest values of both R_a and χ . Moreover, both parameters

Table 3 Hansen solubility parameters for PVDF and the tested solvents

	δ_d (MPa ^{1/2})	δ_h (MPa ^{1/2})	δ_h (MPa ^{1/2})	R_a	χ
PVDF	17.20	12.50	9.20	—	—
DMS	17.19	7.78	10.55	4.91	0.32
DMG	17.17	6.91	9.94	5.64	0.47
DMA	17.15	6.21	9.42	6.29	0.66

δ_d : dispersion forces, δ_h : polar force, δ_h : hydrogen force, χ : Flory–Huggins interaction parameter.



increased with the length of the solvent backbone chain, indicating a gradual reduction in compatibility between the polymer and the solvent. These results are consistent with the experimental observations presented in the phase diagrams (Fig. 1), as discussed below.

Fig. 1a shows the Hansen solubility sphere, which suggests that only DMS should in principle be able to dissolve PVDF. However, this expectation was not borne out by experiment:

PVDF did not dissolve in any of the three solvents at room temperature. This outcome is consistent with previous reports suggesting that solubility parameter calculations provide only rough estimates of solvating power rather than exact measurements.²⁴ The solvating power of the DBEs increased with the temperature, enabling dissolution of the PVDF and the formation of a clear homogeneous polymer solution. Phase separation then occurred upon cooling the resulting solutions. The

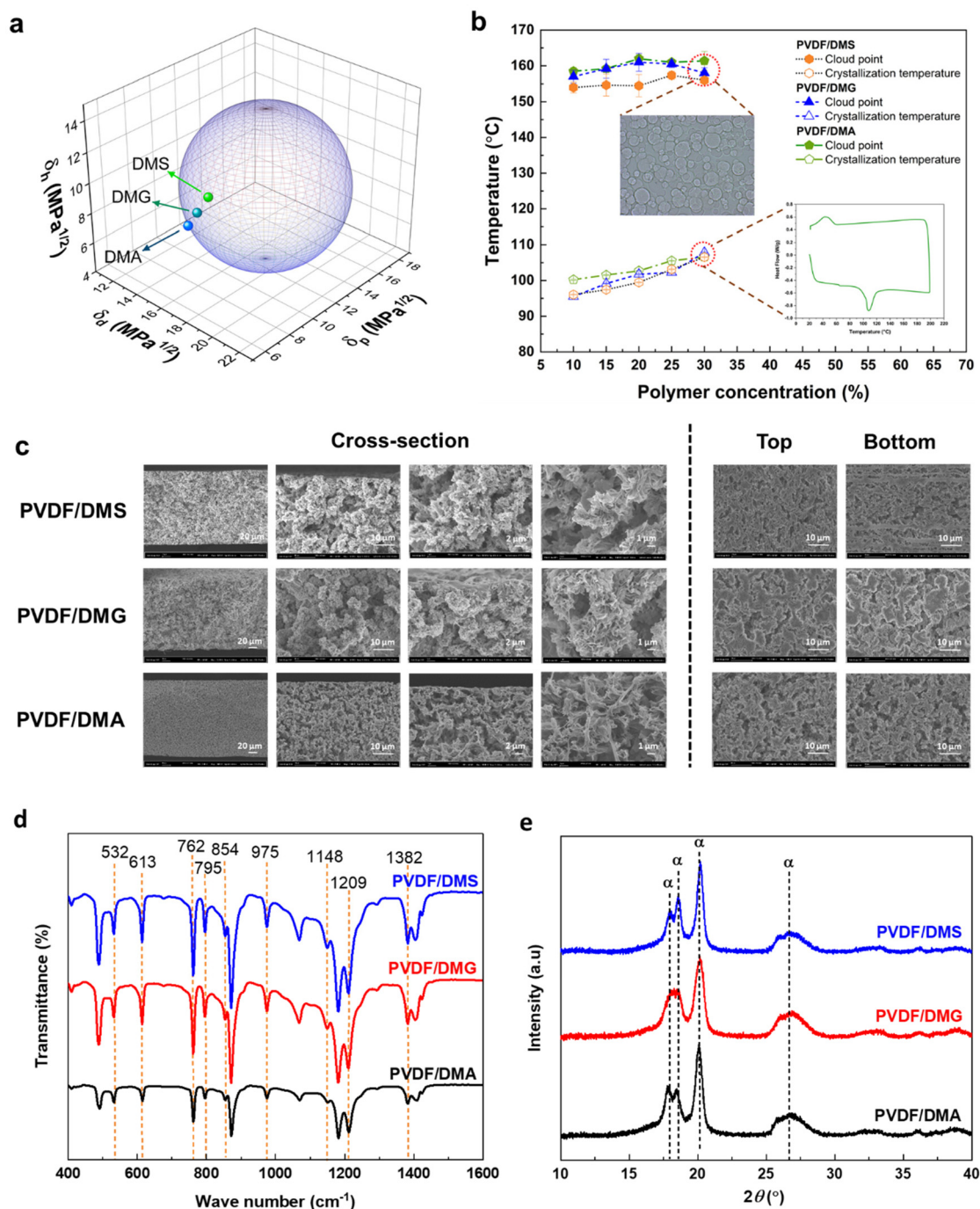


Fig. 1 (a) Solubility sphere of PVDF in Hansen space together with the positions of the three solvents examined in this work (DMS, DMG and DMA). (b) Cloud points and crystallization temperatures of PVDF/DMS, PVDF/DMG and PVDF/DMA. (c) Cross-sections and upper and lower face morphologies of the fabricated membranes. (d) FTIR spectra and (e) XRD patterns of membranes fabricated in DMS, DMG, and DMA.



new solvents should thus permit membrane fabrication using the TIPS approach, like other environmentally friendly solvents that have been used in PVDF membrane fabrication.

Fig. 1b presents a phase diagram showing the cloud point and crystallization temperature vary as functions of the polymer concentration for polymer concentrations between 10 wt% and 30 wt%. Remarkably, there are no intersections between the cloud point and crystallization curve (monotectic point) throughout this concentration range. This indicates that all of the studied PVDF/solvent systems underwent liquid-liquid phase separation at polymer concentrations below 30 wt%. Membranes formed by such phase separation processes would be expected to have a coherent and interconnected structural morphology, and could thus offer outstanding performance in diverse applications.

The phase diagrams also reveal a clear trend in cloud point temperatures: as the solvent alkyl chain length increases, the compatibility between PVDF and the solvent falls, causing the cloud point to shift towards higher temperatures. This is consistent with the previously discussed trends in the Hansen solubility and Flory–Huggins parameters.

3.2. Membrane properties

Fig. 1c and S1† present cross-sectional views and the morphologies of the upper and lower faces of PVDF membranes fabricated using the three tested DBE solvents. The SEM images showed that all of the prepared membranes had bicontinuous structures with interconnected cellular voids throughout their cross-sections together with sheaf-like structures on their top and bottom surfaces. This morphology indicates a predominantly L–L phase separation process, in accordance with the phase diagram presented in Fig. 1b. As can be seen in Fig. 1b the cloud points temperatures are higher than the crystallization temperatures indicating that the polymer-solvent will experience the L–L phase separation. In this method the polymer solution separates to polymer-rich and polymer-lean phases, resulting in PVDF with a bicontinuous structure. Moreover, the membranes have a uniform porous structure throughout and can thus be classified as symmetric membranes. This symmetry together with their interconnected voids and sheaf-like structures should increase their permeability and selectivity, making them interesting candidates for use in diverse membrane processes including membrane distillation. Fig. 1d shows the FTIR spectra of PVDF membranes fabricated with the tested DBE solvents. The spectra exhibit distinct transmittance peaks at 532, 613, 762, 795, 854, 975, 1148, 1209, and 1382 cm^{-1} , indicating that all membranes consist predominantly of the α -phase PVDF polymorph. To verify the crystalline structure of the fabricated PVDF membranes, they were analyzed by XRD. The resulting XRD patterns (see Fig. 1e) have 2θ peaks at angles of 17.6, 18.3, 19.9, and 26.6 degrees, which is characteristic of α -phase PVDF, in accordance with the FTIR data. Moreover, the XRD patterns had no discernible peaks associated with the β and γ phases, indicating that the prepared membranes consist exclusively of α -phase PVDF.

The formation of a pure α -phase crystal in the PVDF membranes can be attributed to the dipole moment of the solvents used in this study, which are reportedly below 3 Debye.⁴⁷ When PVDF dissolves in a solvent with a low dipole moment solvent, there are minimal interactions between the solvent and the PVDF polymer chain. This causes the PVDF chains to form unexpanded or shrunken globules, leading to the formation of the α -phase crystal.⁴⁸ Conversely, solvents with higher dipole moments (*e.g.*, cyclic carbonates) interact more strongly with the PVDF chain, leading to the adoption of a zig-zag configuration that favors the formation of the β -phase.²⁴ It is worthwhile to consider that in both case scenarios, the solvent dissolves the PVDF polymer. Yet, the strength of the interaction dictates whether the chain orientation in the PVDF polymer occurs or not.

Fig. 2a shows the tensile strength and elongation at break of the fabricated PVDF membranes. It is clear that the three DBE solvents had differing effects on the membrane's mechanical properties: the PVDF/DMA membrane had the highest tensile strength, while the PVDF/DMG membrane had the lowest tensile strength and elongation at break. The superior mechanical properties of the PVDF/DMA and PVDF/DMS membranes can primarily be attributed to their interconnected bicontinuous structure, which extends throughout their cross-sections. This bicontinuous structure facilitates the effective distribution of external forces applied to the membrane, thereby enhancing its mechanical strength. The PVDF/DMG membrane has a comparatively low tensile strength and elongation at break because it has a higher mean pore size (Fig. 2f) and a less interconnected structure than the PVDF/DMA and PVDF/DMS membranes.

Fig. 2b compares the mechanical strength of the membranes prepared in this work to that of previously reported PVDF flat sheet membranes fabricated using polymer solutions with concentrations of 15 wt% to 25 wt%. It is clear that the use of biodegradable DBE solvents yields membranes with greater mechanical strength than those prepared with both conventional toxic solvents and previously reported environmentally friendly alternatives. The higher mechanical strength reported in dibutyl phthalate (DBP) can be attributed to the significantly higher polymer concentration. In this context it is worth noting that while phthalates containing plasticizers are widely used to prepare PVDF membranes *via* TIPS,^{49–52} these substances have strong adverse effects on human health and environment.^{20,53,54}

Fig. 2c–f provide detailed information on the surface roughness, pore size, porosity, contact angle, thickness, and liquid entry pressure of the prepared membranes. All of the fabricated membranes exhibit high porosity ($\approx 79\%$), indicating the presence of significant void volumes within the membrane structure. Furthermore, altering the solvent used in the fabrication process did not substantially change the membranes' overall porosity.

The contact angle measurements showed that all of the newly fabricated membranes had high contact angles. As the DBEs used in this study are water-soluble, the prepared membranes were thoroughly washed with water to remove any



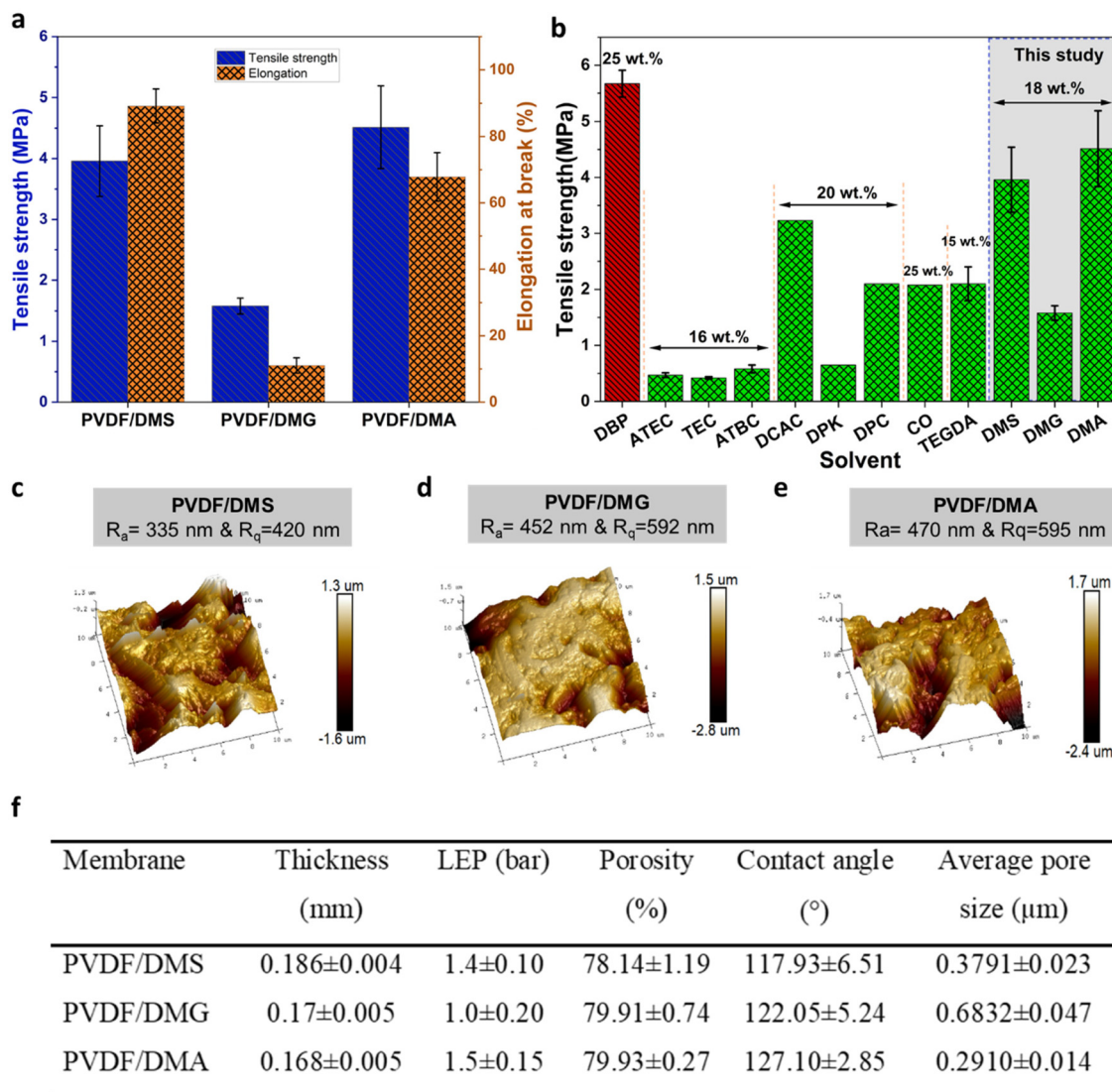


Fig. 2 (a) Tensile strength and elongation at break values of the prepared membranes, (b) comparison of the tensile strength of the PVDF membranes prepared in this study to that of previously reported PVDF flat sheet membranes prepared from polymer solutions with concentrations of 15 wt% to 25 wt% (PVDF/DBP,⁵⁵ PVDF/ATEC,²² PVDF/TEC,²² PVDF/ATBC,²² PVDF/DCAC,²⁶ PVDF/DPK,⁵⁶ PVDF/DPC,⁵⁷ PVDF/CO,⁵⁸ PVDF/TEGDA³⁴). (c), (d), and (e) AFM and surface roughness data for PVDF/DMS, PVDF/DMG, and PVDF/DMA membranes, respectively, (f) thickness, liquid entry pressure (LEP), porosity, contact angle, and mean pore size values of the prepared membranes.

residual solvents. Consequently, the final membranes consisted solely of pure PVDF, which is inherently hydrophobic. The differences in the membranes' hydrophobicity can thus be attributed to differences in their surface roughness; the contact angle increased in parallel with the alkyl chain length of the DBE solvents (see Fig. 2c–e). It should be noted that further experiments using DBE solvents with longer alkyl chains will be needed to draw a definitive conclusion about the relationship between chain length and membrane hydrophobicity. However, increasing the alkyl chain length may also reduce the solvating power of the DBE solvent, which would in turn affect the conditions needed for membrane fabrication and the accessibility of the solvent, making it hard to evaluate the impact of longer chains in practice.

The liquid entry pressure (LEP) is a key membrane property in MD processes; it is essential to ensure that the operating pressure remains below the LEP to avoid pore wetting and a loss of membrane selectivity. The LEP values of the prepared membranes are presented in Fig. 2f, which shows that the PVDF/DMG membrane had the highest pore size and the lowest LEP, while the PVDF/DMA membrane had the lowest pore size and the highest LEP.

3.3. Membrane distillation performance

The performance of the three prepared membranes was initially evaluated using an air gap membrane distillation (AGMD) setup with feed temperatures of 50 $^\circ\text{C}$ to 80 $^\circ\text{C}$ and a fixed flow rate of 1.50 L min⁻¹. Fig. 3a shows that the fluxes of



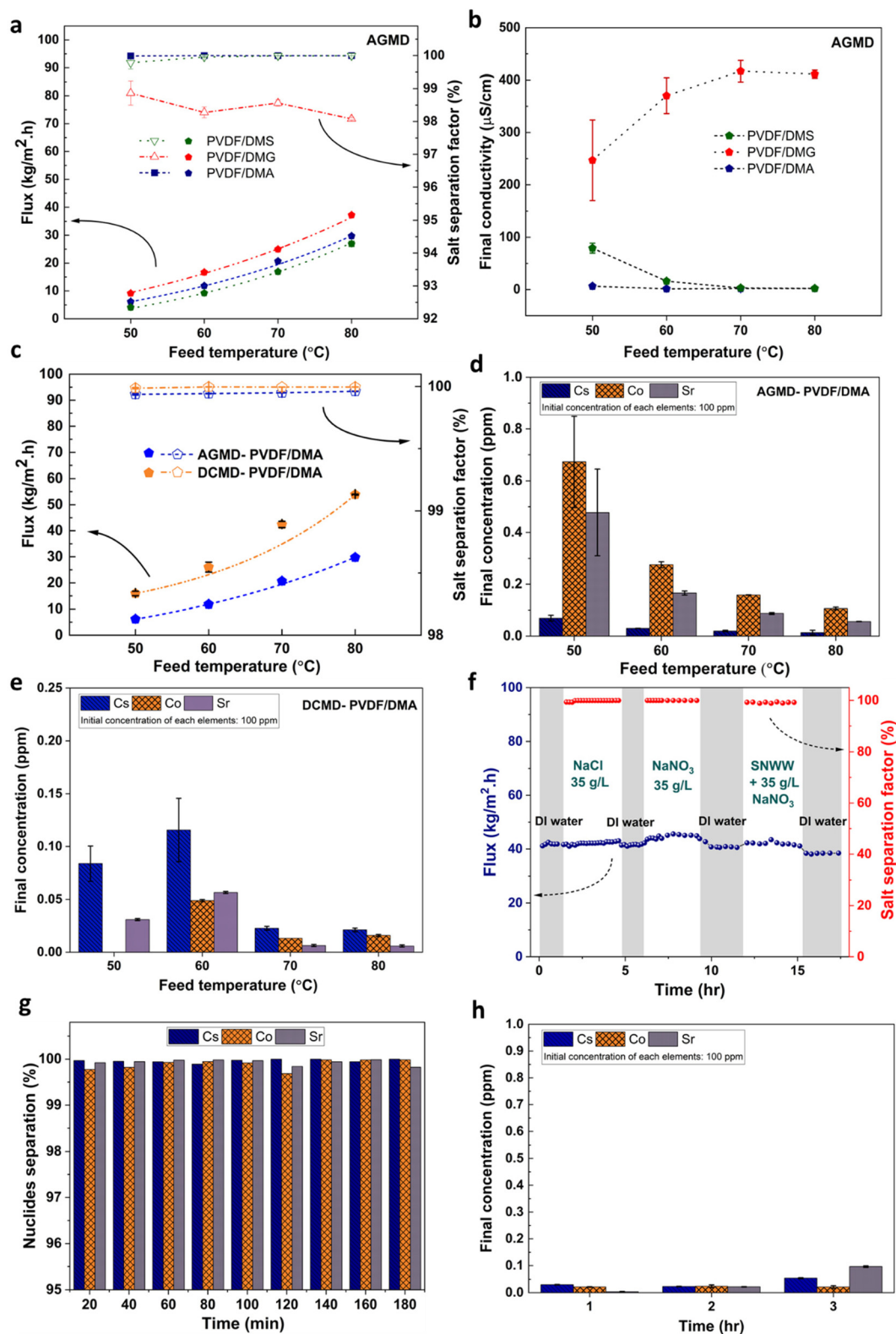


Fig. 3 (a) Flux and salt rejection of the prepared membranes when exposed to a 35 g L⁻¹ NaCl feed solution in AGMD. (b) Final permeate conductivities for PVDF/DMS, PVDF/DMG, and PVDF/DMA membranes in the AGMD configuration. (c) AGMD and DCMD performance of PVDF/DMA membranes using SNWW in 35 g L⁻¹ NaNO₃. (d) Final concentrations of nuclides (Cs⁺, Co²⁺, and Sr²⁺) in the AGMD permeate. (e) Final concentrations of nuclides (Cs⁺, Co²⁺, and Sr²⁺) in the DCMD permeate. (f) Stability of PVDF/DMA membranes in extended experiments using feed solutions of 35 g L⁻¹ NaCl, 35 g L⁻¹ NaNO₃, and SNWW containing 35 g L⁻¹ NaNO₃. (g) Nuclide separation performance of the PVDF/DMA membrane in terms of rejection percentage (%). (h) Final concentrations of Cs⁺, Co²⁺, and Sr²⁺ in the permeate during the final 3 hours of the long-term stability experiment.



all three membranes increased exponentially with the feed temperature. The PVDF/DMG membrane achieved the highest permeate flux ($37.3 \text{ kg m}^{-2} \text{ h}^{-1}$) while maintaining a salt separation factor above 98%. However, the final conductivity of the PVDF/DMG membrane permeate exceeded $200 \mu\text{S cm}^{-1}$ at a feed temperature of 50°C and increased to above $400 \mu\text{S cm}^{-1}$ at higher feed temperatures (70°C and 80°C) (see Fig. 3b). Thus, although the PVDF/DMG membrane achieved high AGMD performance in terms of permeate flux, its separation efficiency was poor and the conductivity of its permeate exceeded the upper limit recommended by the World Health Organization (WHO) ($400 \mu\text{S cm}^{-1}$). This outcome is consistent with the fact that the PVDF/DMG membrane had the largest average pore size of those prepared in this work (Fig. 2f).

The PVDF membrane prepared using DMA as the solvent had more favorable membrane performance, with both high flux ($29.7 \text{ kg m}^{-2} \text{ h}^{-1}$ at 80°C) and good separation efficiency (Fig. 3a and b); the final conductivity of the permeate from this membrane was around $1 \mu\text{S cm}^{-1}$.

The PVDF/DMA membrane had a higher separation factor than the PVDF/DMG membrane because of its smaller mean pore size. Moreover, it achieved a higher flux than the PVDF/DMS membrane ($26.9 \text{ kg m}^{-2} \text{ h}^{-1}$ at 80°C) because of its lower membrane thickness, which facilitates vapor transport across the membrane. The PVDF/DMA membrane was therefore selected for evaluation in the decontamination of synthetic nuclear wastewater (SNWW).

SNWW decontamination was performed under a range of operating conditions with feed temperatures of 50°C to 80°C while the permeate temperature was maintained at 20°C . The results obtained (see Fig. 3c) revealed that both AGMD and DCMD membrane fluxes increased with the feed temperature; the permeate flux in the AGMD configuration reached $29.2 \text{ kg m}^{-2} \text{ h}^{-1}$ at 80°C , while a significantly higher maximum of $53.5 \text{ kg m}^{-2} \text{ h}^{-1}$ was achieved in the DCMD configuration. This difference can be attributed to the different mass transfer mechanisms in AGMD and DCMD. In AGMD, vapor is transported from the permeate side to the condensation surface *via* natural convection within the air gap, driven by the temperature difference between the two sides of the membrane. However, the need for the vapor to cross an air barrier reduces the permeate flux significantly. Conversely, in DCMD the permeate liquid is in direct contact with the permeate side of the membrane, so the vapor does not have to cross an air gap. This enables a higher permeate flux than is possible in AGMD.

Fig. 3d and e show that the PVDF/DMA membranes achieved good performance in nuclide removal from SNWW in both DCMD and AGMD configurations: the nuclide concentrations in the permeate were below 0.7 parts per million (ppm), compared to around 100 ppm in the initial SNWW.

The PVDF/DMA membranes exhibited excellent flux and a high rejection capability in DCMD experiments, and had better mechanical properties than the other membranes (Fig. 2a and b). Therefore, to evaluate their practical utility in nuclear wastewater treatment, experiments were conducted to determine the stability of their performance and their resis-

tance to fouling and degradation in the DCMD configuration. Multiple feed solutions were used for this purpose, starting with distilled water to ensure that the membranes were defect-free and exhibited no leakage. The membranes were then tested with solutions containing 35 g L^{-1} NaCl and NaNO_3 , followed by SNWW containing 35 g L^{-1} NaNO_3 . In all cases, the temperatures of the feed solution and permeate were maintained at 70°C and 20°C , respectively.

As shown in Fig. 3f, the PVDF/DMA membrane had a stable flux throughout the experiment, indicating low susceptibility to fouling. Moreover, it achieved outstanding rejection capabilities, maintaining a rejection rate above 99.5% for the 35 g L^{-1} NaCl and NaNO_3 solutions. After being operated for 12 hours under these conditions, the feed solution was changed to SNWW containing 35 g L^{-1} NaNO_3 . The flux remained above $40 \text{ kg m}^{-2} \text{ h}^{-1}$ when using the SNWW, with no significant reduction in the removal of NaNO_3 salt, indicating that the presence of the nuclides did not adversely affect the membrane's performance. Furthermore, the PVDF/DMA membrane achieved high nuclide removal efficiency, with removal rates of 99.96% for Cs^+ , 99.90% for Co^{2+} , and 99.93% for Sr^{2+} .

The MD results show that the PVDF/DMA membrane performs well in SNWW decontamination, with exceptional flux rates and high stability over the course of the experiments. To further characterize the membrane's capabilities, a comparative analysis was conducted by benchmarking the obtained results against reported results for commercially available MD membranes and membranes prepared in lab-scale studies (see Table 4). This revealed that the PVDF/DMA membrane was outstanding in several aspects. First, it achieved a substantially higher flux ($42.40 \text{ kg m}^{-2} \text{ h}^{-1}$) than any other membrane when using a 35 g L^{-1} NaCl feed solution. Second, it displayed excellent salt rejection capabilities, with removal rates above 99.9% for both NaCl and NaNO_3 . Finally, it demonstrated effective nuclide separation capabilities, demonstrating its suitability for treating nuclear wastewater. Together with its favorable mechanical properties (see Fig. 2), these results show that the PVDF/DMA system is a very promising option for the sustainable fabrication of membranes to be used in decontaminating nuclear wastewater by DCMD.

The exceptional separation performance and mechanical properties of the PVDF/DMA membrane can be attributed to the favorable properties of the green DBE solvent, which shifted the monotectic point of the polymer/solvent system upwards with respect to the polymer concentration, allowing phase inversion to occur by L-L phase separation. This resulted in the formation of a membrane with a bicontinuous structure that confers outstanding performance.

As mentioned in the introduction section, green solvents must be readily available in large quantities at reasonable prices to be practically useful. Fig. 4, therefore, shows the costs of conventional toxic solvents and previously reported green solvents for PVDF membrane fabrication. It has been noted that NMP and DMF, which are commonly used solvents for TIPS and NIPS processes, tend to be relatively expensive compared to other solvents, particularly toxic ones, despite their



Table 4 Performance of selected membranes in nuclear wastewater treatment by MD

Membrane material	Solvent	Configuration	Condition	Separation performance	Flux (kg m ⁻² h ⁻¹)	Ref.
Commercial PP (Wochi, WHPP96-21, China)	—	HF (VMD)	T_f : 70 °C	Co (11 ppm): $R = 99.67$ – 99.82%	6.30	59
Commercial PP (Wochi, WHPP96-21, China)	—	HF (VMD)	T_f : 70 °C	Sr (10 ppm): $R = 99.74$ – 99.6%	6.71	60
PES	NMP	FS (DCMD)	T_f : 55 °C	^{60}Co , ^{137}Cs , ^{85}Sr (1 mS cm ⁻¹): $R > 99.5\%$	0.16	10
PS	NMP	—	T_p : 21.5 °C	^{60}Co , ^{137}Cs , ^{85}Sr (1 mS cm ⁻¹): $R > 99.5\%$	0.08	
Commercial TF200	—	—	—	^{60}Co , ^{137}Cs , ^{85}Sr (1 mS cm ⁻¹): $R > 99.5\%$	0.15–0.16	
Commercial PTFE	—	HF (VMD)	T_f : 90 °C	Cs(i) (20 ppm): $R \approx 99.98\%$	6.82	9
Commercial PVDF	—	HF (DCMD)	T_f : 47.5 °C	Cs ⁺ , Sr ²⁺ , Co ²⁺ (20, 100 ppm): $R \approx 100\%$ (DF = 10 ⁵)	19.00	11
Commercial PP	—	FS (DCMD)	T_p : 27 °C	100 g L ⁻¹ NaNO ₃ : $R > 99\%$ Co ²⁺ , Sr ²⁺ , Cs ⁺ (100 ppm): DF = 10 ⁵ 50 g L ⁻¹ NaNO ₃ : $R = 99.4\%$ 5000 mg L ⁻¹ B: $R = 99.7\%$	8.3 0	12
PVDF	NMP	FS (DCMD)	T_f : 70 °C	Cr (450 ppm): $R = 99.98\%$	19.70	8
	DMAC	—	T_p : 20 °C	Co (450 ppm): $R = 99.97\%$		
	DMF	—	—	Cs (450 ppm): $R = 99.85\%$	15.46	
	—	—	—	35 g L ⁻¹ NaCl: $R > 99.5\%$		
PVDF	DMA	FS (DCMD)	T_f : 70 °C	35 g L ⁻¹ NaNO ₃ : $R > 99.5\%$	11.24	
	—	—	T_p : 20 °C	Cs (100 ppm): $R = 99.96\%$ Co (100 ppm): $R = 99.90\%$ Sr (100 ppm): $R = 99.93\%$ 35 g L ⁻¹ NaCl: $R > 99.9\%$ 35 g L ⁻¹ NaNO ₃ : $R > 99.9\%$	42.40	This study

PP: polypropylene, PES: polyethersulfone, PS: polysulfone, PTFE: polytetrafluoroethylene, NMP: *N*-methyl pyrrolidone, DMAC: *N,N*-dimethyl acetamide, DMF: dimethyl formamide, DMA: dimethyl adipate, FS: flat sheet, HF: hollow fiber, VMD: vacuum membrane distillation, DCMD: direct contact membrane distillation, T_f : feed temperature, T_p : permeate temperature, B: boron, DF: decontamination factor, R: rejection.

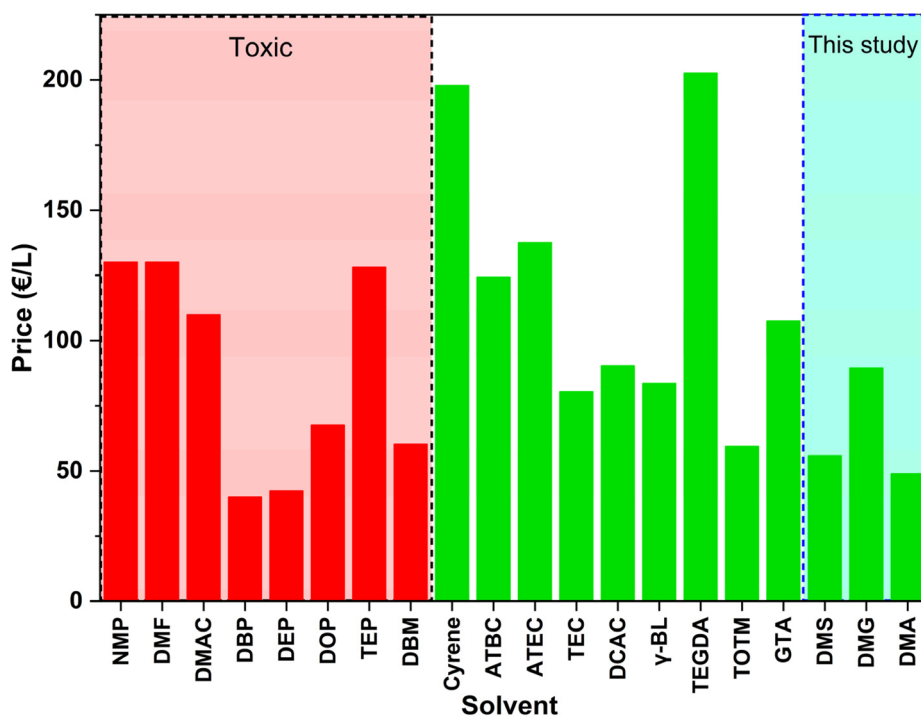


Fig. 4 Price comparison of the selected toxic and non-toxic solvents for PVDF membrane fabrication via TIPS processes. Prices were obtained from the website of Sigma-Aldrich (<https://www.sigmaaldrich.com/SE/en>) and TCI chemicals (<https://www.tcichemicals.com/SE/en>) Sweden in June 2023.



favorable solvating properties. In contrast, the solvent employed in this work, DMA, was the most economical of the considered green solvents. This cost advantage further emphasizes its attractiveness as a green solvent for membrane fabrication.

4. Conclusion

The results presented here demonstrate the potential of dibasic ester solvents – specifically, DMS, DMG, and DMA – as biodegradable non-toxic options for PVDF membrane fabrication. Phase diagram analysis showed that the use of these solvents shifts the monotectic point of the PVDF/solvent system towards higher polymer concentrations, thereby enabling the formation of membranes *via* a L–L phase inversion mechanism. This resulted in the formation of a unique bicontinuous structure, which was confirmed by SEM to be present throughout the membranes' entire cross-section. Furthermore, measurements of the membranes' mechanical properties showed that they displayed outstanding mechanical strength, ranking among the best reported PVDF flat sheet membranes in this respect. A notable advantage of these membranes over those prepared using both green and toxic solvents is their bicontinuous structure, which effectively distributes external forces within the membrane and thus contributes to this good mechanical performance.

In MD experiments, the best performing membrane (PVDF/DMA) exhibited exceptional performance with a stable flux of approximately $42 \text{ kg m}^{-2} \text{ h}^{-1}$ and a consistent rejection rate of 99.9% for 35 g L^{-1} NaCl and NaNO_3 feed solutions over an 18-hour testing period. This flux value exceeds those reported for other PVDF membranes under comparable conditions, emphasizing the remarkable efficiency of the PVDF/DMA membrane. The PVDF/DMA membrane also achieved high rejection factors for three common radionuclides (Cs^+ , Co^{2+} , and Sr^{2+}), highlighting its potential utility in nuclear wastewater decontamination by MD.

DBEs are available on large scales at prices that are below those of toxic solvents and comparable to those of recently reported green solvents. Given the outstanding properties of the membranes obtained using these solvents, they are well positioned for use in industrial-scale membrane production.

Abbreviations

AFM	Atomic force microscopy
AGMD	Air gap membrane distillation
ATBC	Tributyl <i>O</i> -acetyl citrate
ATEC	Acetyl triethyl citrate
CO	Cyclohexanone
Cyrene	Dihydrolevoglucosenone
DBE	Dibasic ester
DBM	Maleic acid dibutyl ester
DBP	Dibutyl phthalate

DCAC	Diethyleneglycol monoethyl ether acetate
DCMD	Direct contact membrane distillation
DEP	Diethyl phthalate
DMF	Dimethyl formamide
DMS	Dimethyl succinate
DMG	Dimethyl glutarate
DMA	Dimethyl adipate
DMAC	<i>N,N'</i> -Dimethyl acetamide
DPC	Diphenyl carbonate
DPK	Diphenyl ketone
ECTFE	Ethylene-chlorotrifluoroethylene
FESEM	Field emission scanning electron microscope
FTIR	Fourier-transform infrared spectroscopy
GTA	Glycerol triacetate
ICP-OES	Inductively coupled plasma optical emission spectrometer
MD	Membrane distillation
NIPS	Non-solvent induced phase separation
NMP	<i>N</i> -Methyl pyrrolidone
PES	Polyether sulfone
Polarclean	Methyl-5-(dimethylamino)-2-methyl-5-oxopentanoate
PP	Polypropylene
PS	Polysulfone
PTFE	Polytetrafluoroethylene
PVDF	Polyvinylidene fluoride
SNWW	Simulated nuclear wastewater
TBC	Tributyl citrate
TEC	Triethyl citrate
TEGDA	Triethylene glycol diacetate
TIPS	Thermal induced phase separation
TOTM	Trioctyl trimellitate
TEP	Triethyl phosphate
γ -BL	γ -Butyrolactone
FS	Flat sheet
HF	Hollow fiber
VMD	Vacuum membrane distillation
XRD	X-ray diffraction

Symbols

A	Effective filtration area of membrane (m^2)
C_p	Final concentration in the feed solution (g L^{-1})
C_f	Initial concentration in the permeate solution (g L^{-1})
F	Tensile force (N)
J	permeate water flux ($\text{kg m}^{-2} \text{ h}^{-1}$)
L	Length of the membrane after broken (cm)
L_0	Initial length of the membrane (cm)
m_d	Weights of the dry membranes (g)
m_w	Weights of the wet membranes (g)
LEP	liquid entry pressure (bar)
R	Gas constant ($8.3145 \text{ J mol}^{-1} \text{ K}^{-1}$)
R_a	Solubility parameter distance
R_s	Surface roughness (nm)
R_q	Root mean square roughness (nm)
T	Temperature (K)



T_C	Crystallization temperature ($^{\circ}\text{C}$)
T_f	Feed inlet temperature ($^{\circ}\text{C}$)
T_p	Permeate inlet temperature ($^{\circ}\text{C}$)
V	Collected permeate (kg)
V_s	Molar volume of the solvent ($\text{cm}^3 \text{mol}^{-1}$)
t	Time (h)
α	Salt rejection factor (%)
δ	Solubility parameter ($\text{MPa}^{1/2}$)
δ_d	Dispersion force ($\text{MPa}^{1/2}$)
δ_p	Polar force ($\text{MPa}^{1/2}$)
δ_h	Hydrogen bond force ($\text{MPa}^{1/2}$)
ϵ	Overall porosity (%)
σ	Tensile strength (MPa)
ρ_p	Density of polymer (g cm^{-3})
ρ_k	Density of kerosene (g cm^{-3})
χ	Flory–huggins interaction parameter

Conflicts of interest

There are no conflicts to declare.

Acknowledgements

The authors would like to express their appreciation for the financial support provided by the Kempe Foundation (JCK22-0008). We also extend our gratitude to Professor Solomon Tesfalidet for his assistance with ICP measurements. Furthermore, we acknowledge the financial support received from the National Natural Science Foundation of China (22078146) and the Natural Science Foundation of Jiangsu Province (BK20200091).

References

- 1 A. Adamantiades and I. Kessides, *Energy Policy*, 2009, **37**, 5149–5166.
- 2 N. Öztürk, D. Kavak and T. E. Köse, *Desalination*, 2008, **223**, 1–9.
- 3 G. Zakrzewska-Trznadel, M. Harasimowicz and A. G. Chmielewski, *Sep. Purif. Technol.*, 2001, **22–23**, 617–625.
- 4 J. Wang and C. Chen, *Biotechnol. Adv.*, 2009, **27**, 195–226.
- 5 M. Jiang, Z. Fang, Z. Liu, X. Huang, H. Wei and C.-Y. Yu, *Cleaner Eng. Technol.*, 2023, **12**, 100589.
- 6 A. H. Englert and J. Rubio, *Int. J. Miner. Process.*, 2005, **75**, 21–29.
- 7 M. R. Awual, S. Suzuki, T. Taguchi, H. Shiwaku, Y. Okamoto and T. Yaita, *Chem. Eng. J.*, 2014, **242**, 127–135.
- 8 M. Essalhi, N. Ismail, S. Tesfalidet, J. Pan, Q. Wang, Z. Cui, M. C. García-Payo, M. Khayet, J.-P. Mikkola, S. Sarmad, D. Bouyer, Y. Zhao, B. Li, C. André Ohlin and N. Tavajohi, *Chem. Eng. J.*, 2022, **446**, 137300.
- 9 X. Jia, L. Lan, X. Zhang, T. Wang, Y. Wang, C. Ye and J. Lin, *Sep. Purif. Technol.*, 2021, **275**, 119129.
- 10 M. Khayet, *Desalination*, 2013, **321**, 60–66.
- 11 H. Liu and J. Wang, *J. Hazard. Mater.*, 2013, **261**, 307–315.
- 12 X. Wen, F. Li and X. Zhao, *Desalination*, 2016, **394**, 101–107.
- 13 G. Zakrzewska-Trznadel, M. Harasimowicz and A. G. Chmielewski, *J. Membr. Sci.*, 1999, **163**, 257–264.
- 14 A. Alkhudhiri, N. Darwish and N. Hilal, *Desalination*, 2012, **287**, 2–18.
- 15 Z. Cui, E. Drioli and Y. M. Lee, *Prog. Polym. Sci.*, 2014, **39**, 164–198.
- 16 M. Khayet and T. Matsuura, *Ind. Eng. Chem. Res.*, 2001, **40**, 5710–5718.
- 17 U. Basak, M. Pakhira, S. Sahoo, S. Majumdar, R. Ghosh, J. Kundu, T. Ghosh, T. Ghosh, A. K. Nandi and D. P. Chatterjee, *ACS Appl. Polym. Mater.*, 2022, **4**, 5756–5771.
- 18 P. Yadav, N. Ismail, M. Essalhi, M. Tysklind, D. Athanassiadis and N. Tavajohi, *J. Membr. Sci.*, 2021, **622**, 118987.
- 19 N. T. Hassankiadeh, Z. Cui, J. H. Kim, D. W. Shin, S. Y. Lee, A. Sanguineti, V. Arcella, Y. M. Lee and E. Drioli, *J. Membr. Sci.*, 2015, **479**, 204–212.
- 20 Z. Cui, N. T. Hassankiadeh, S. Y. Lee, J. M. Lee, K. T. Woo, A. Sanguineti, V. Arcella, Y. M. Lee and E. Drioli, *J. Membr. Sci.*, 2013, **444**, 223–236.
- 21 J. F. Kim, J. T. Jung, H. H. Wang, S. Y. Lee, T. Moore, A. Sanguineti, E. Drioli and Y. M. Lee, *J. Membr. Sci.*, 2016, **509**, 94–104.
- 22 S.-i. Sawada, C. Ursino, F. Galiano, S. Simone, E. Drioli and A. Figoli, *J. Membr. Sci.*, 2015, **493**, 232–242.
- 23 N. T. Hassankiadeh, Z. Cui, J. H. Kim, D. W. Shin, A. Sanguineti, V. Arcella, Y. M. Lee and E. Drioli, *J. Membr. Sci.*, 2014, **471**, 237–246.
- 24 N. Ismail, M. Essalhi, M. Rahmati, Z. Cui, M. Khayet and N. Tavajohi, *Green Chem.*, 2021, **23**, 2130–2147.
- 25 W. Ma, Z. Zhou, N. Ismail, E. Tocci, A. Figoli, M. Khayet, T. Matsuura, Z. Cui and N. Tavajohi, *J. Membr. Sci.*, 2023, **669**, 121303.
- 26 L. Wang, D. Huang, X. Wang, X. Meng, Y. Lv, X. Wang and R. Miao, *Desalination*, 2015, **361**, 25–37.
- 27 M. Liu, Z.-l. Xu, D.-g. Chen and Y.-m. Wei, *Desalin. Water Treat.*, 2010, **17**, 183–192.
- 28 D. Mullette and H. J. Muller, *Membranes halar*, WO2003068374A1, 2003.
- 29 S. Rajabzadeh, T. Maruyama, Y. Ohmukai, T. Sotani and H. Matsuyama, *Sep. Purif. Technol.*, 2009, **66**, 76–83.
- 30 S. Rajabzadeh, M. Teramoto, M. H. Al-Marzouqi, E. Kamio, Y. Ohmukai, T. Maruyama and H. Matsuyama, *J. Membr. Sci.*, 2010, **346**, 86–97.
- 31 N. Ghasem, M. Al-Marzouqi and A. Duaidar, *Int. J. Greenhouse Gas Control*, 2011, **5**, 1550–1558.
- 32 N. Ghasem, M. Al-Marzouqi and A. Duidar, *Sep. Purif. Technol.*, 2012, **98**, 174–185.
- 33 N. Ghasem, M. Al-Marzouqi and N. Abdul Rahim, *Sep. Purif. Technol.*, 2012, **99**, 91–103.



- 34 Z. Cui, N. T. Hassankiadeh, S. Y. Lee, K. T. Woo, J. M. Lee, A. Sanguineti, V. Arcella, Y. M. Lee and E. Drioli, *J. Membr. Sci.*, 2015, **473**, 128–136.
- 35 Z. Cui, S. Xu, J. Ding, J. Zhang, B. He, H. Wang and J. Li, *Polymers*, 2018, **10**, 719.
- 36 G. Liu, J. Pan, X. Xu, Z. Wang and Z. Cui, *J. Membr. Sci.*, 2020, **612**, 118375.
- 37 A. Bottino, G. Camera-Roda, G. Capannelli and S. Munari, *J. Membr. Sci.*, 1991, **57**, 1–20.
- 38 M. R. M. Abed, S. C. Kumbharkar, A. M. Groth and K. Li, *J. Membr. Sci.*, 2012, **407–408**, 145–154.
- 39 Z. Song, M. Xing, J. Zhang, B. Li and S. Wang, *Sep. Purif. Technol.*, 2012, **90**, 221–230.
- 40 N. E. Kob, in *Clean Solvents*, American Chemical Society, 2002, ch. 17, vol. 819, pp. 238–253.
- 41 M. Watch, Dibasic Ester (DBE) Market is Booming in Near Future 2023–2028, <https://www.marketwatch.com/press-release/dibasic-ester-dbe-market-is-booming-in-near-future-2023-2028-2023-03-14>, (accessed 25 May, 2023).
- 42 A. K. Dikshit and A. K. Nandi, *Macromolecules*, 1998, **31**, 8886–8892.
- 43 A. K. Dikshit and A. K. Nandi, *Macromolecules*, 2000, **33**, 2616–2625.
- 44 D. Dasgupta and A. K. Nandi, *Macromolecules*, 2005, **38**, 6504–6512.
- 45 N. Ismail, J. Pan, M. Rahmati, Q. Wang, D. Bouyer, M. Khayet, Z. Cui and N. Tavajohi, *J. Membr. Sci.*, 2022, **646**, 120238.
- 46 Y. Tang, Y. Lin, W. Ma and X. Wang, *J. Membr. Sci.*, 2021, **639**, 119759.
- 47 A. Abe, *J. Am. Chem. Soc.*, 1984, **106**, 14–19.
- 48 T. Nishiyama, T. Sumihara, E. Sato and H. Horibe, *Polym. J.*, 2017, **49**, 319–325.
- 49 X. Li, Y. Wang, X. Lu and C. Xiao, *J. Membr. Sci.*, 2008, **320**, 477–482.
- 50 X. Lu and X. Li, *J. Appl. Polym. Sci.*, 2009, **114**, 1213–1219.
- 51 S. Rajabzadeh, C. Liang, Y. Ohmukai, T. Maruyama and H. Matsuyama, *J. Membr. Sci.*, 2012, **423–424**, 189–194.
- 52 G.-L. Ji, L.-P. Zhu, B.-K. Zhu, C.-F. Zhang and Y.-Y. Xu, *J. Membr. Sci.*, 2008, **319**, 264–270.
- 53 J. C. Lamb, R. E. Chapin, J. Teague, A. Davis Lawton and J. R. Reel, *Toxicol. Appl. Pharmacol.*, 1987, **88**, 255–269.
- 54 M. Ema, A. Harazono, E. Miyawaki and Y. Ogawa, *J. Appl. Toxicol.*, 1997, **17**, 223–229.
- 55 J.-H. Zuo, C. Wei, P. Cheng, X. Yan, Y. Chen and W.-Z. Lang, *J. Membr. Sci.*, 2020, **604**, 118089.
- 56 Y. Tang, Y. Lin, W. Ma, Y. Tian, J. Yang and X. Wang, *J. Appl. Polym. Sci.*, 2010, **118**, 3518–3523.
- 57 Y. Lin, Y. Tang, H. Ma, J. Yang, Y. Tian, W. Ma and X. Wang, *J. Appl. Polym. Sci.*, 2009, **114**, 1523–1528.
- 58 Y. Su, C. Chen, Y. Li and J. Li, *J. Macromol. Sci., Part A: Pure Appl. Chem.*, 2007, **44**, 305–313.
- 59 F. Jia, Y. Yin and J. Wang, *Prog. Nucl. Energy*, 2018, **103**, 20–27.
- 60 F. Jia, J. Li, J. Wang and Y. Sun, *Ann. Nucl. Energy*, 2017, **103**, 363–368.

